Multimed Tools Appl (2018) 77:22671–22688
DOI 10.1007/s11042-017-5146-3

Preliminary study on angiosperm genus classification by weight decay and combination of most abundant color index with fractional Fourier entropy

Yu-Dong Zhang[1,2,3] · **Junding Sun**[1]

Received: 23 June 2017 / Revised: 13 August 2017 / Accepted: 22 August 2017 /
Published online: 2 September 2017

Abstract In order to develop an efficient angiosperm-genus classification system, we first collected petal image of Hibiscus, Orchis, and Prunus, by digital camera, and remove the backgrounds by region-growing method. Next, we proposed a novel feature-extraction method, which combined most abundant color index (MACI) and introduced the fractional Fourier entropy (FRFE). Third, we submitted the 41 features to a single-hidden layer feedforward neural-network (SLFN), with weight decay (WD) to avoid overfitting. The 10 × 10-fold cross validation showed our method achieved an overall accuracy of 98.92%. Without weight decay, the overall accuracy decreased to 95.50%. Our experiments validated that optimal decay factor is 0.1, and optimal number of hidden neurons is 15. This proposed method is excellent. It performs better than six state-of-the-art approaches and AlexNet. The weight decay helps to enhance generalization of our classifier.

Keywords Angiosperm genus · Weight decay · Classification · Fractional fourier entropy · Feature extraction · Most abundant color index · Color histogram · Single-hidden layer feed-forward neural-network · Petal image · AlexNet

1 Introduction

Angiosperm are flowering plants with 416 families and 295,383 species [29]. Both angiosperms and gymnosperms [6] are seed-producing plants, Nevertheless, the former has

Yu-Dong Zhang and Junding Sun contributed equally to this work.

✉ Yu-Dong Zhang
yudongzhang@ieee.org

[1] School of Computer Science and Technology, Henan Polytechnic University, Jiaozuo, Henan 454000, People's Republic of China

[2] Translational Imaging Division & MRI Unit, Columbia University and New York State Psychiatric Institute, New York, NY 10032, USA

[3] Department of Informatics, University of Leicester, Leicester LE1 7RH, UK

distinctive features [26]: flowering organs, endosperm within the seeds, and producing fruits covering the seeds.

The flowering organs (i.e., flowers) are the most remarkable feature [3]. It provides the plant with a more species-specific breeding system [31], which guarantees a ready means into different species without crossing back into related species. The faster speciation ability make them adaptive to wider ranges of ecological niches [21].

Most of people cannot identify them due to the enormous species (over 250,000) [13]. They need to turn to specialists, read flower monographs, or search the internet, in order to identify the families, genera, and species of the flowers [2]. A feasible means is by computer vision based on a digital camera either in hand or in a mobile-phone [19]. Scholars have shown increasing interest in this field.

In the last decade, Saitoh, Aoki and Kaneko [28] focused the blooming flowers and defocused the background. They selected a route to extract the boundary. Their method is the combination of normalized cost (NC) and piecewise linear discriminant (PLD). Their aim is minimize the sum of local cost divided by the route length. Nilsback and Zisserman [22] developed a visual vocabulary (VV) method. They used the nearest neighbor classifier (NNC). Nilsback and Zisserman [23] computed three features: (i) hue-saturation-value (HSV), (ii) Scale-invariant feature transform (SIFT), and (iii) histogram of oriented gradient (HOG). Afterwards, they used support vector machine (SVM) as the classifier. Guru, Sharath and Manjunath [14] extracted features from gray-level co-occurrence matrix (GLCM) and Gabor filter response (GFR). They employed k-nearest neighbors (KNN) algorithm. Guru, Sharath Kumar and Manjunath [15] improved their methods later. They introduced a new color texture moment (CTM), and replaced KNN with probabilistic neural network (PNN). Cheng and Tan [8] combined 100 SIFT features, 40 pyramid histogram of oriented gradient (PHOG) features, and 64 color histogram features. They used sparse representation-based classifier (SRC). Sari and Suciati [30] took only a^* and b^* channel (ABC) in the $L^*a^*b^*$ color space. They also obtained texture features by segmentation-based fractal texture analysis (SFTA). They used kNN classifier with cosine distance. Vasudevan, Joshi, Shekokar, Kumar, Kumar and Guru [35] obtained the flower skeletons, and then used Delaunay triangulation (DT) to extract features. They used symbolic classifier (SC).

Meanwhile, there are some apps to identify flowers on either IOS or android platforms. For example, the "Plant Snapp", "Like Thar Garden", "Garden Answers Plant Identification", "Flower Checker", "Plantifier", etc. Nevertheless, those apps are mainly based on color and shape features. For the petals with similar color and shape, those apps may perform bad.

This study proposed a new color feature – most abundant color index (MACI) and used a relatively new texture feature—fractional Fourier entropy (FRFE). This combined feature set showed promising result. In the classification stage, we used the single-hidden layer feedforward neural-network (SLFN), and used the weight decay technique to avoid overfitting.

The highlights of this study are composed of four points: (i) We proposed a hybrid feature combining MACI and FRFE, and showed the superiority of combined features than individual feature. (ii) We used weight decay for generalization, and our experiment showed the effectiveness of weight decay. (iii) Our method gives better performance than six state-of-the-art approaches and AlexNet. (iv) Grid searching was used to find the optimal parameters of our classifier.

The rest of the paper is described as follows: Section 2 contains the angiosperm dataset containing three genera as Hibiscus, Orchis, and Prunus. Section 3 provides the proposed most

abundant color index and introduces fractional Fourier entropy. It also gives the background of classifier and weight decay. Section 4 provides the experiment results and discussions. Final Section 4.1 gives the concluding remarks.

2 Materials

We collected three genera of flower petals (Hibiscus, Orchis, and Prunus). Each contains 40 images. The flowers are collected in the nature in China. We put them under a glass over a piece of black cloth, making them spread all the way. The images were captured with a digital Canon EOS 80D camera. The CMOS image sensors can take 24.2 megapixels with 3:2 aspect ratio. A 1/8000 s shutter was set. Shutter lag time was 0.06 s.

There are different species within each genus. The scale, pose, and light illumination vary in each image. Original size of each image is 6000 × 4000. Region-growing method [27] was carried out to remove the background automatically. Original captured picture is too large and contains a massive of redundant spatial information. After removing the background, we placed the petal in the center, and resized the image size of 400 × 400.

Figure 1 shows the samples of the petal images. In the light of improving the generalization of the classification system, the petal images were captured in different rotations, angles, and illumination conditions. We did not carry out any scale normalization, pose normalization, or illumination compensation. The reason is we would like our classifier has the ability to resist scale change, pose variation, and illumination variation.

3 Methodology

3.1 Most abundant color index

Color histogram (CH) [16] was employed in this study; nevertheless, it contains 64 features and most of them are close to zero [1]. Therefore, we proposed a new color feature scheme, which extracts the indexes of several most abundant color channels. This new scheme is named most abundant color index (MACI).

We firstly discretized the color space from the original 256 × 256 × 256 = 16,777,216 color space to 4 × 4 × 4 = 64 discrete color bins [36]. We counted pixel number in each of the 64

Fig. 1 Samples of the petal image dataset: **a** Hibiscus, **b** Orchis, and **c** Prunus

bins. Fig. 2(a) shows an original rose image in RGB space. Figure 2(b) shows the 64 discrete color bins. Figure 2(c) shows the color histogram of rose image. The y-axis denotes the number of pixels, and the x-axis denotes the 64 color bin index. Figure 2(d) shows the sorted color histogram. The x-axis now denotes the index. We can observe the five indexes are 53, 58, 57, 52, and 32, respectively.

The pseudocode of calculating MACI is listed in Algorithm 1. Here we choose five most abundant indexes by experiences. The advantages of MACI contain two points. First, it can extracts color information of any type of given color images. Second, it uses less features than color histogram.

Algorithm 1 Pseudocode of MACI.

Step 1 Import the petal image.
Step 2 Transform it to gray-scale image.
Step 3 Perform 36 different FRFTs with rotation angles shown in Figure 4.
Step 4 Calculate Shannon entropy over the 36 FRFT spectrums.

3.2 Fractional fourier entropy

Suppose $x(t)$ denotes a signal in time or spatial domain, then the corresponding fractional Fourier transform (abbreviated as FRFT) [7] is defined below:

$$F_a(u) = \int_{-\infty}^{\infty} x(t)\mathscr{K}(t,u|a)\mathrm{d}t \tag{1}$$

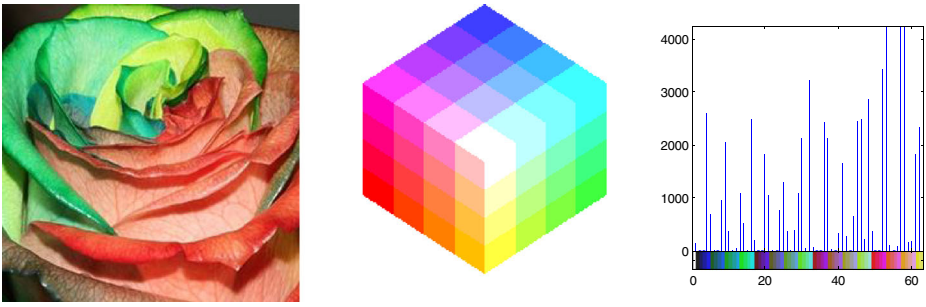

(a) Rose Image (b) 64 Discrete Bins (c) Color Histogram

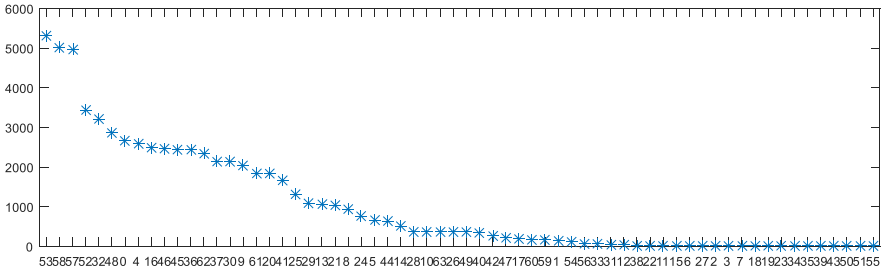

(d) Sorted Color Histogram

Fig. 2 Sorted color histogram of a rose image

here u represents the frequency domain [4] a the angle of FRFT $\mathscr{S}$ is the transform kernel as:

$$\mathscr{S}(t,u|a) = \sqrt{1-j\cot a} \times \exp\left(j\pi\left(t^2\cot a - 2ut\csc a + u^2\cot a\right)\right) \tag{2}$$

Here j represents the imaginary unit, and exp.(.) represents the exponential function. From basic mathematical knowledge, we know that if a is set the value of a multiple of π, then both "csc" and "cot" operators will diverge to infinity [10]. Using knowledge of limitation, we can transform Eq. (2) to

$$\mathscr{S}(t,u|a) = \begin{cases} \mathcal{C}(t-u) \\ \sqrt{1-j\cot a}\exp\left(j\pi\left(t^2\cot a - 2ut\csc a + u^2\cot a\right)\right) \\ \mathcal{C}(t+u) \end{cases} if \ \frac{a}{\pi} \begin{cases} = 2k \\ \neq k \\ = (2k+1)\pi \end{cases} \tag{3}$$

where k represents an arbitrary integer, and C is the Dirac delta function.

An illustration of FRFT over the rectangular function is plotted in Fig. 3. The rectangular function $r(t)$ is defined with

$$r(t) = \begin{cases} 0 \\ 1 \\ 1/2 \end{cases}, if \ |t| \begin{cases} > \\ < \\ = \end{cases} \frac{1}{2} \tag{4}$$

Here |.| represents the absolute value. The FRFT results of $r(t)$ with angles a of 0/10, 2/10, 4/10, 6/10, 8/10, and 10/10 are shown in Fig. 3(a-f), respectively.

When FRFT extends to the two-dimensional situation, we have two angles: a for x-axis and denoted by b for y-axis. This combined angle vector (a, b) serve as the rotation angle for 2D–FRFT. In this study, we chose by experiences in total 36 different 2D–FRFTs as shown in Fig. 4. That means, we chose 36 angle vectors, i.e., (0, 0), (0, 0.2), …, (0, 1), (0.2, 0), (0.2, 0.2), …, (0.2, 1), …, (1, 0), (1, 0.2), …, (1,1).

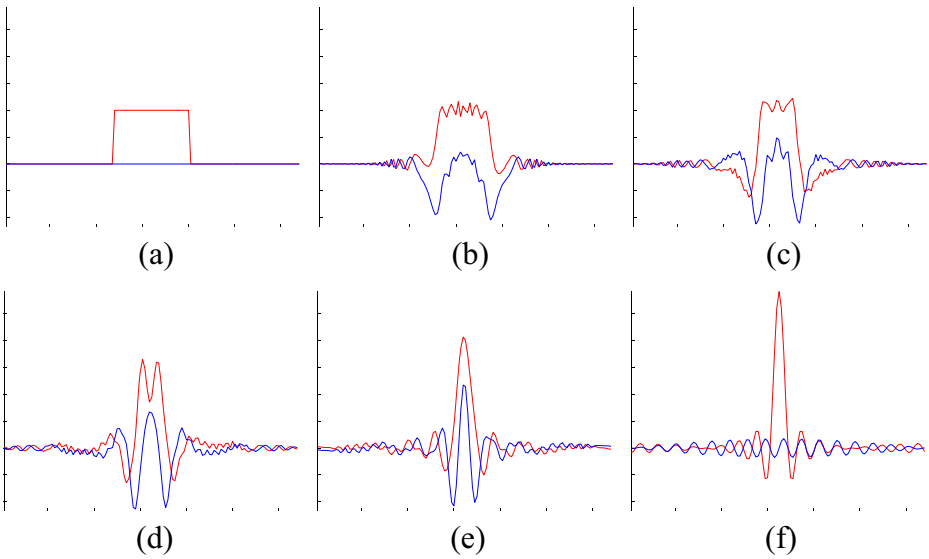

Fig. 3 FRFT curve of $r(t)$: **a** a = 0/10; **b** a = 2/10; **c** a = 4/10; **d** a = 6/10; **e** a = 8/10; **f** a = 10/10. (The red and blue lines denote the real and imaginary parts, respectively)

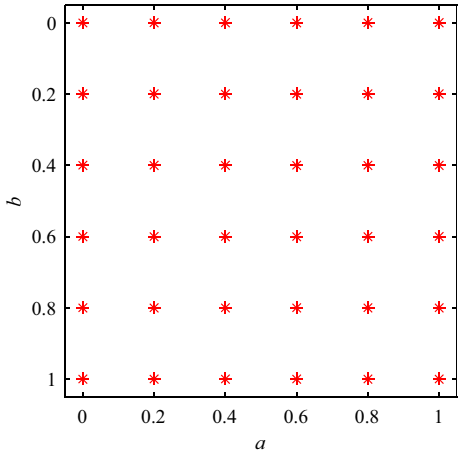

Fig. 4 36 different combinations with their angle vector (a, b) from 0 to 1 with step of 0.2

Yang, Sun, Dong, Liu and Yuan [37] proposed a novel image feature dubbed fractional Fourier entropy (FRFE), which is a combination of fractional Fourier transform with Shannon entropy. Sun [34] applied FRFE in creating an intelligent pathological brain detection system. Cattani and Rao [5] applied FRFE in tea category identification. Those literature all obtained promising results. In this study, we also employed FRFE by calculating Shannon entropy over the 36 FRFT spectrums. The pseudocode of FRFE is presented in Algorithm 2.

Algorithm 2 Fractional Fourier entropy.

Step 1 Import the petal image with RGB color channels.
Step 2 Divide the color space into 64 discrete color bins.
Step 3 Count the pixel numbers in each bin and Calculate the color histogram.
Step 4 Sort the color histogram.
Step 5 Record the five most abundant color indexes.

3.3 Classifier

The 5 MACIs and 36 FRFEs are combined, and then submitted to a single-hidden layer feed-forward neural-network (SLFN). The number of hidden neuron is set to 15 by grid-searching method (See Section 4.9). Thus, a 41–15-3 SLFN was initialized with random weights and biases as shown in Fig. 5.

The SLFN is trained in supervised learning scheme [32]. Suppose the loss function is $E(\omega)$, where ω represents the weights and biases. The backpropagation (BP) learning algorithm [12] can be divided into two phases: (i) propagation and (ii) weight update.

In the propagation stage, we first forward propagated an input through the network and generated an output [25]. Afterwards, we generated the gradient descent by backward propagation [33]. In the weight update stage, the gradient is multiplied with a learning rate η, and the term is subtracted from current weight [11]. In mathematics, the BP can be written as

$$\omega_k \leftarrow \omega_k - \eta \frac{\partial E}{\partial \omega_k} \tag{5}$$

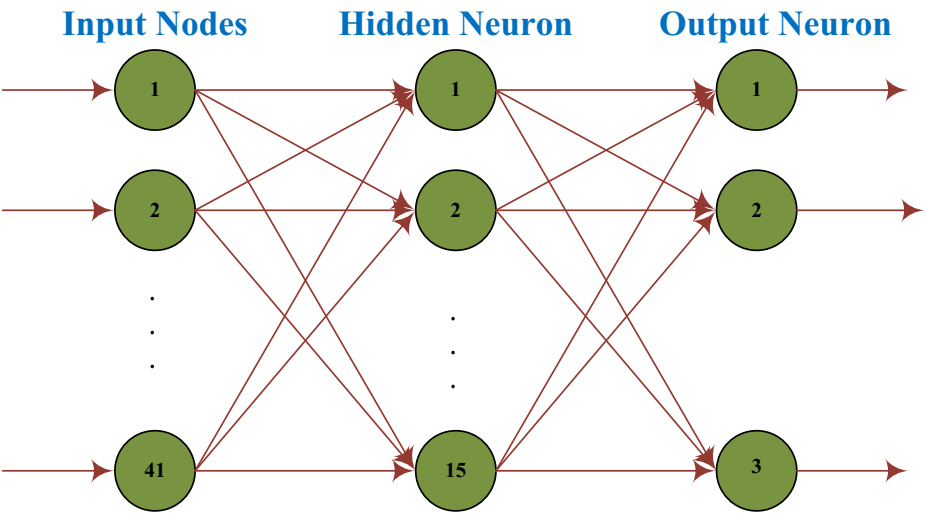

Fig. 5 Structure of SLFN in petal classification

The above procedure repeats until the performance of SLFN meets our termination requirement.

3.4 Weight decay

The "Weight Decay (WD)" [24] is a powerful regularization method that can reduce the test error and resist overfitting, at the expense of increasing training error. A weight decay factor λ was introduced, and the first term of Eq. (5) was multiplied with (1 - λ) as

$$\omega_k \leftarrow (1-\lambda)\omega_k - \eta \frac{\partial E}{\partial \omega_k} \tag{6}$$

where η represents the learning rate, E is the loss function, λ is the weight decay factor, and ω_k represents the weights and biases at k-th step.

The weight decay term modified the learning rate [38], so the new algorithm shrinks the weight vector at each step, before performing the usual weight update in standard BP [20]. In this study, we chose the weight decay factor fixed, namely, unchanged during the training procedure. In addition, we found λ = 0.1 performed the best for our task.

3.5 Experiment design

We did not divide the dataset into training, validation, and test sets. The reason is that our dataset is small, so dividing will yield a smaller training dataset, which is not suitable for training. To get test error without reducing the size of training dataset [18], this study employed a ten-fold cross validation method.

We divide the dataset into ten folds. Each fold contains 4 Hibiscus images, 4 Orchis images, and 4 Prunus images. Then, we used nine folds for training, and the other fold for test. The

performance of trained SLFN over test set was recorded. The above procedure repeated 10 times as shown in Fig. 6. In each time, different sets were chosen as test set [17]. Finally, the performance over each test set was combined and a final overall test performance was presented. To further reduce the variance on test set, we run the 10-fold cross validation 10 times.

The flowchart of our method is provided in Fig. 7. In addition, its pseudocode was described in Algorithm 3.

Algorithm 3 Pseudocode of our proposed system.

Step 1 Import the petal image dataset. Segment the dataset into 10 folds.
Step 2 Extract the most abundant color index features and fractional Fourier entropy features.
Step 3 Initiate a classifier based on single-hidden-layer feed-forward neural network, and use weight decay as the regularization method.
Step 4 Cross Validation, let k = 1.
Step 4.1 Choose k-th fold as test fold, and the other as training folds.
Step 4.2 Train the classifier using the sum of nine training folds.
Step 4.3 Record the result on the test fold.
Step 4.3 k = k+1, jump to Step 4.1.
Step 5 Summarize the results on all test folds, and report the performance.

4 Results and discussions

4.1 Feature extraction

A petal image was used to extract both color feature and texture feature. Figure 8(a) shows the original petal image. Figure 8(b) shows the color histogram of this petal image. Figure 8(c) offers the five MACIs. Obviously, the color vector here is [0, 54, 58, 53, 59].

Then, the texture feature was obtained. The FRFT of the petal image is shown below in Fig. 9. Here the arrangement is coherent with that in Fig. 4. That is, the left-upper subgraph represents the FRFT with (a, b) = (0, 0), and the right-button

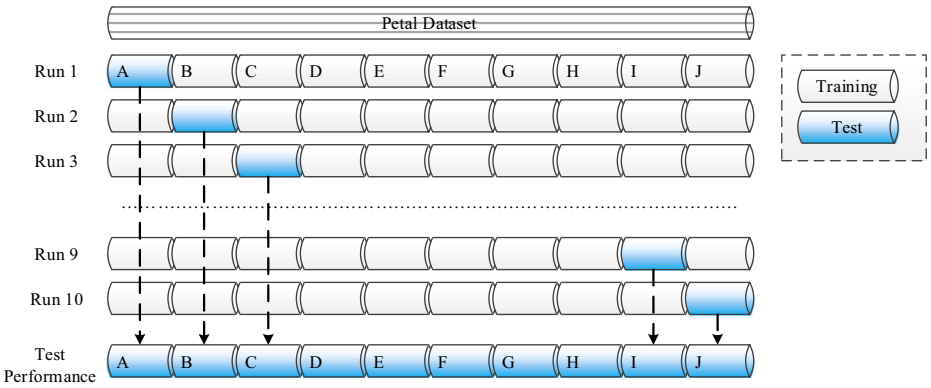

Fig. 6 10-fold cross validation (A-J are 10 folds of petal dataset)

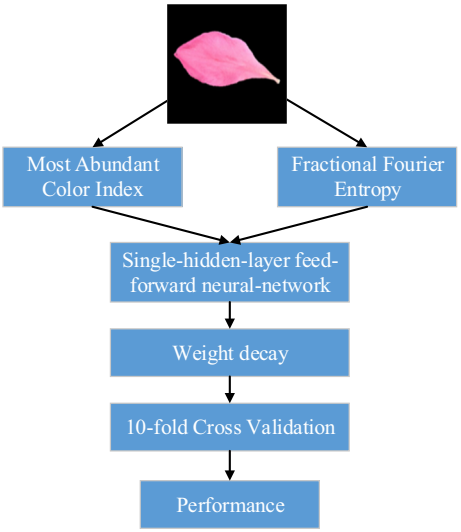

Fig. 7 Flowchart of this proposed method

subgraph corresponds to FRFT with $(a, b) = (1, 1)$. We can deduce that FRFT will provide more information than standard Fourier transform.

4.2 Performance without weight decay

In this experiment, we compared the "SLFN with WD model (SLFN + WD)" with "SLFN without WD". The parameters were the same as previous Section: We run a 10 × 10-fold cross validation. The weight-decay factor λ was set as 0.1. The maximum iteration was 1000. The learning rate η was set as 0.01. The overall accuracy was used as the measure. The comparison results are listed in Table 1.

Table 1 shows that merely SLFN model obtains an overall accuracy of 95.50%; nevertheless, introducing WD can significantly increase the overall accuracy to 98.92%. The increase of 3.41% is under strict statistical analysis of 10 × 10-fold cross validation; hence, the improvement is meaningful. Connor, Hollensen, Krigolson and Trappenberg [9] presented

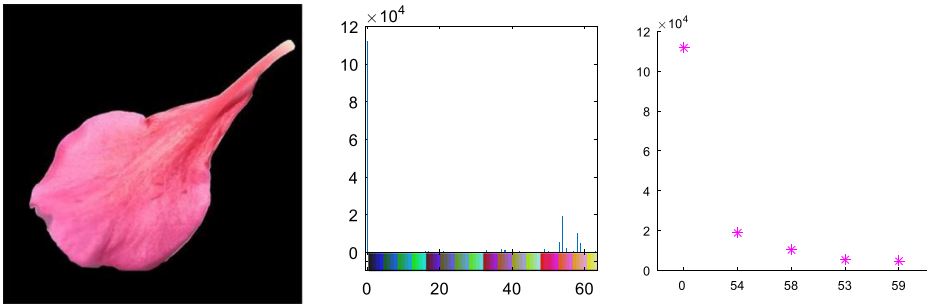

(a) Petal Image (b) Color Histogram (c) Five MACIs

Fig. 8 The MACI features of a petal image

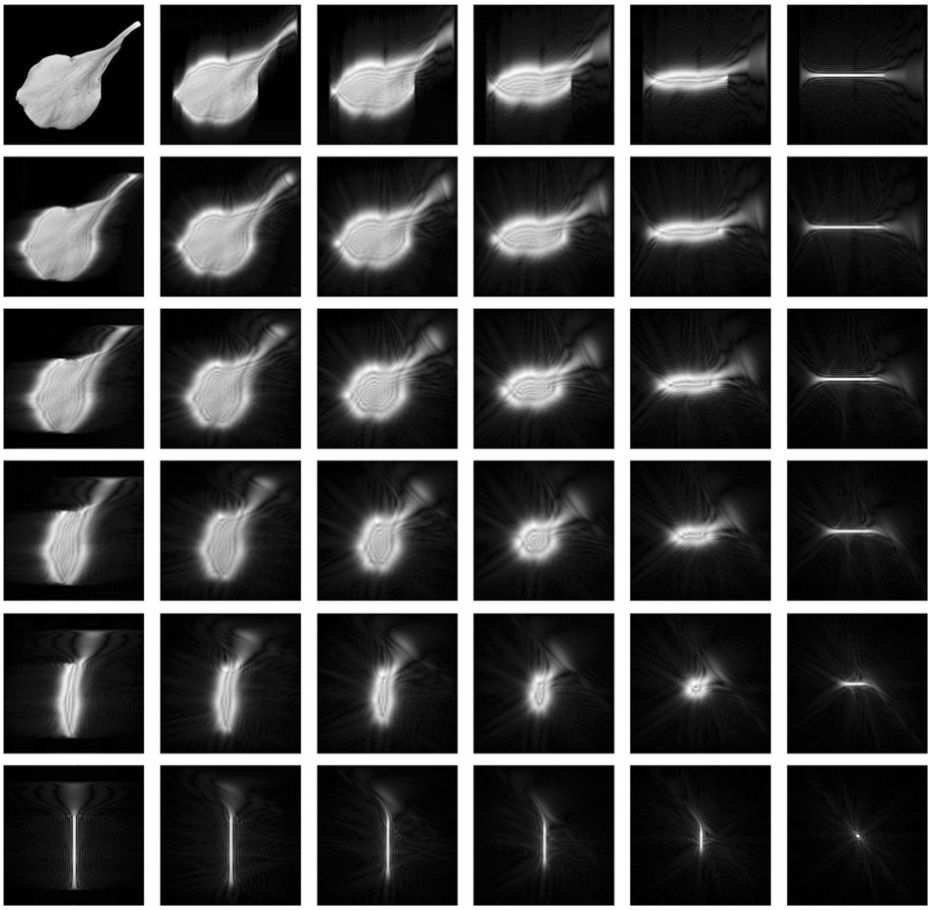

Fig. 9 FRFT of the petal image

Bayesian priors can be implemented in gradient descent as a form of weight decay; hence, we will study their connections in future.

4.3 Classifier comparison

We compared the proposed single-hidden layer feed-forward neural-network with weight decay with traditional classifiers, for example, the decision tree (DT), support vector machine (SVM), and Bayesian classifier (BC). λ was assigned to the value of 0.1, and number of

Table 1 With Weight Decay versus W/O Weight Decay

Method	Overall Accuracy
With WD ($\lambda = 0.1$)	98.92%
W/O WD	95.50%

(W/O = Without)

Table 2 Classifier Comparison

Classifier	Overall Accuracy
DT	96.67%
SVM	96.92%
BC	95.33%
SLFN + WD (Proposed)	98.92%

hidden neurons was assigned to the value of 15. The comparison results are listed in Table 2 and Fig. 10.

Here DT, SVM, and BC are not combined with WD, since their training algorithms have already taken overfitting into account. The results in Table 2 and Fig. 10 showed that DT, SVM, and BC yielded an overall accuracy of 96.67%, 96.92%, and 95.33%, respectively. Those three traditional classifiers perform worse than our proposed "SLFN + WD" classifier. The reason is two folds: First, the universal approximation theory guaranteed SLFN can approximate to any function. Second, the weight decay shows an excellent ability in resisting overfitting as in Section 4.2.

4.4 In-depth statistical analysis

Table 3 lists the results over 10 runs of 10-fold cross validation. Here *x*-*y*-*z* represents *x*, *y*, and *z* instances are classified correctly as Class 1 (Hibiscus), Class 2 (Orchis), and Class 3 (Prunus) respectively. *x*(*y*) represents *x* instances of all classes are recognized correctly out of *y* instances.

The results in Table 3 show the identification result of each fold in each run. As remembered, there are in total 40 petal images of Hibiscus, 40 of Orchis, and 40 of Prunus. Hence, we have 4 instance of each class in every fold. The 10-fold cross validation was repeated 10 times; hence, we identify correctly in total 396, 394, and 397 instances of Hibiscus, Orchis, and Prunus, respectively. The final averaged overall accuracy is 98.92%.

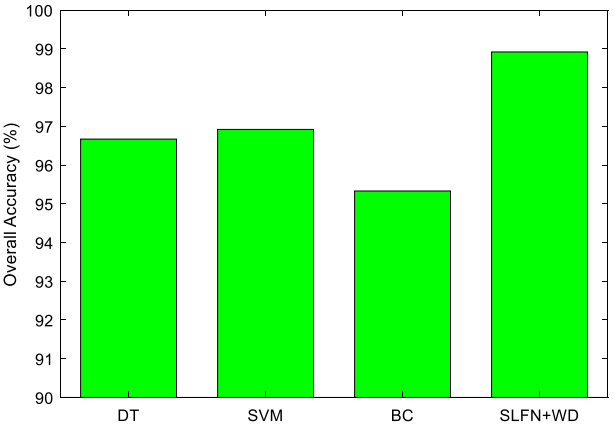

Fig. 10 Plot of overall accuracy comparison of four different classifiers

Table 3 Results over 10 runs of 10-fold cross validation

	F1	F2	F3	F4	F5	F6	F7	F8	F9	F10	Total	Acc.
R1	4–4-4	4–4-4	4–4-4	4–4-4	4–4-4	4–4-4	4–4-4	4–4-4	4–4-4	3–4-4	39–40-40	99.17%
	12(12)	12(12)	12(12)	12(12)	12(12)	12(12)	12(12)	12(12)	12(12)	11(12)	119(120)	
R2	4–4-4	4–4-4	3–4-4	4–4-4	3–4-4	3–4-4	4–4-4	4–4-4	4–4-4	4–3-4	37–39-40	96.67%
	12(12)	12(12)	11(12)	12(12)	11(12)	11(12)	12(12)	12(12)	12(12)	11(12)	116(120)	
R3	4–4-4	4–3-4	4–3-4	4–4-4	4–4-4	4–4-3	4–4-4	4–4-4	4–4-4	4–4-4	40–38-39	97.50%
	12(12)	11(12)	11(12)	12(12)	12(12)	11(12)	12(12)	12(12)	12(12)	12(12)	117(120)	
R4	4–4-4	4–4-4	4–4-4	4–4-4	4–4-4	4–4-4	4–4-4	4–4-4	4–4-4	4–4-4	40–40-40	100.00%
	12(12)	12(12)	12(12)	12(12)	12(12)	12(12)	12(12)	12(12)	12(12)	12(12)	120(120)	
R5	4–4-4	4–4-4	4–4-4	4–4-4	4–4-4	4–4-4	4–4-4	4–4-4	4–4-4	4–4-4	40–40-40	100.00%
	12(12)	12(12)	12(12)	12(12)	12(12)	12(12)	12(12)	12(12)	12(12)	12(12)	120(120)	
R6	4–4-4	4–4-4	4–4-4	4–4-4	4–4-4	4–4-3	4–4-4	4–4-4	4–4-4	4–4-4	40–40-39	99.17%
	12(12)	12(12)	12(12)	12(12)	12(12)	11(12)	12(12)	12(12)	12(12)	12(12)	119(120)	
R7	4–4-4	4–4-4	4–4-4	4–4-4	4–4-4	4–4-4	4–4-4	4–4-4	4–4-4	4–4-4	40–40-40	100.00%
	12(12)	12(12)	12(12)	12(12)	12(12)	12(12)	12(12)	12(12)	12(12)	12(12)	120(120)	
R8	4–3-4	4–4-4	4–4-4	4–4-4	4–4-4	4–4-4	4–4-4	4–4-4	4–4-4	4–4-4	40–39-40	99.17%
	11(12)	12(12)	12(12)	12(12)	12(12)	12(12)	12(12)	12(12)	12(12)	12(12)	119(120)	
R9	4–4-4	4–4-4	4–4-4	4–4-4	4–3-4	4–4-4	4–4-4	4–4-4	4–4-4	4–4-3	40–39-39	98.33%
	12(12)	12(12)	12(12)	12(12)	11(12)	12(12)	12(12)	12(12)	12(12)	11(12)	118(120)	
R10	4–4-4	4–4-4	4–4-4	4–4-4	4–4-4	4–4-4	4–3-4	4–4-4	4–4-4	4–4-4	40–39-40	99.17%
	12(12)	12(12)	12(12)	12(12)	12(12)	12(12)	11(12)	12(12)	12(12)	12(12)	119(120)	
											396–394–397	98.92%
											1187(1200)	

(F = Fold; R = Run)

Remembering that there are different species within each genus, and the photographing conditions (scale, pose, and light illumination) vary in each image. Therefore, this result indicates our method is insensitive to changes of scale, pose, and illumination.

4.5 Comparison to state-of-the-art methods

We compared the proposed MACI + FRFE + SLFN-WD with six state-of-the-art methods: NC + PLD [28], VV + NNC [22], HSV + SIFT + HOG + SVM [23], CTM + GLCM + GFR + PNN [15], ABC + SFTA + KNN [30], and DT + SC [35]. The detailed results are shown in Fig. 11.

Here NC + PLD [28] yields an accuracy of 91%, VV + NNC [22] yields an accuracy of 81.3%, HSV + SIFT + HOG + SVM [23] yields an accuracy of 72.8%, CTM + GLCM + GFR + PNN [15] yields an accuracy of 79%, ABC + SFTA + KNN [30] yields an accuracy of 73.63%, DT + SC [35] yields an accuracy of 93%. In addition, our method outperforms other six methods with an accuracy of 98.92%. This suggests the effectiveness of our proposed MACI and FRFE methods.

Feature is also an important indicate, which measures the efficiency of feature extraction. NC + PLD [28] extracted in total 10 features, ABC + SFTA + KNN [30] extracted 58 features, and other literature did not report the number of features. In contrary, our method only used in total 41 features. This shows the size of our features is moderate. It may be reduced in further studies.

4.6 Comparison to AlexNet

In this experiment, we compared our method with AlexNet [39], which is a well-pretrained 25-layer neural network in the field of deep learning. The AlexNet model in Matlab is trained on a subset of ImageNet database, and it can classify 1000 object categories (for instance, pencil, mouse, keyboard, etc.). We invoked the model by Matlab command of “alexnet”, and

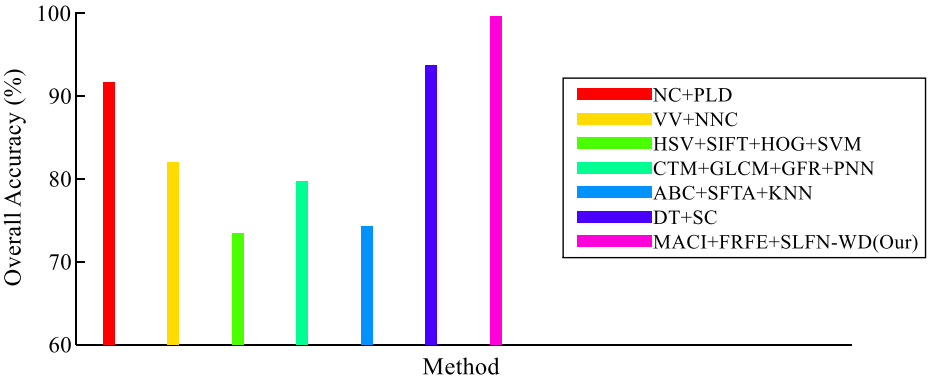

Fig. 11 Comparison to state-of-the-art methods in terms of petal recognition. The accuracies are 91%, 81.3%, 72.8%, 79%, 73.63%, 93%, and 98.92%. (NC = normalized cost, PLD = piecewise linear discriminant; VV = visual vocabulary, NNC = nearest neighbor classifier, HSV = hue saturation value, SIFT = scale-invariant feature transform, HOG = histogram of oriented gradient, SVM = support vector machine, CTM = color texture moment, GLCM = gray level co-occurrence matrix, GFR = Gabor filter response, PNN = probabilistic neural network, ABC = a^* and b^* channels, SFTA = segmentation-based fractal texture analysis, KNN = k-nearest neighbors, DT = Delaunay triangulation, SC = symbolic classifier)

Table 4 Comparison to AlexNet

Method	Overall Accuracy
AlexNet [39]	96.08
MACI + FRFE + SLFN-WD (Our)	98.92%

compared it with our method. The parameter settings were the same as previous experiments. The comparison results are presented in Table 4.

Here we see that AlexNet [39] gives an overall accuracy of only 96.08%, less than our "MACI + FRFE + SLFN-WD" method of 98.92%. The reason is three folds. First, AlexNet [39] can identify 1000 types of objects, but they are not trained particularly for petal identification. Second, the input size of AlexNet [39] is 227 × 227 × 3, we need to resize the original image to 227 × 227, and this low-resolution may impair the information contained in original image. Hence, our method can give better performance than AlexNet.

4.7 Analysis on combined features

The combined features include 5 most abundant color index (MACI) values and 36 fractional Fourier entropy (FRFE) values. In this experiment, we compared the combined feature vector (41 features) with two individual feature vectors: (i) 5 MACIs; (ii) 36 FRFEs. We used SLFN as the classifier and weight decay as the regularization methods. The statistical analysis described in Section 3.5 was used. The results are listed below in Table 5.

The comparison results in Table 5 show that the overall accuracy is only 95.25% when we only used 5 MACIs, and the overall accuracy is 97.33% when we only used 97.33%. Nevertheless, if we combined the two feature sets, the combined features yield an overall accuracy of 98.92%. This result validates the effectiveness of our proposed combined feature vector.

4.8 Optimal weight decay factor

In order to obtain the optimal weight decay factor, here we run a 10 × 10-fold cross validation. The weight decay factor λ was chosen as [0.05, 0.1, 0.15, 0.2, 0.25, 0.3, 0.35, 0.4]. The maximum iteration was 1000. The learning rate η was set as 0.01. The overall accuracy was used as the measure. Figure 12 plots the curve between overall accuracy versus the factor λ.

From the curve in Fig. 12, we can observe that the overall accuracy achieves the highest at the optimal weight decay factor with λ of 0.1. Besides, we see the accuracy has a decreasing trend when λ increases. The reason is when λ is large, the weight update term, viz., the first

Table 5 Combined feature vector versus individual feature vector

Feature Set	Overall Accuracy
5 MACIs	95.25%
36 FRFEs	97.33%
5 MACIs +36 FRFEs (Proposed)	98.92%

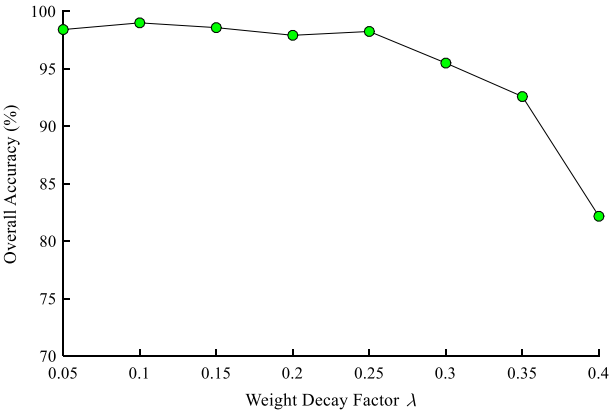

Fig. 12 Optimal Weight Decay Factor

term in Eq. (6), cannot preserve the update rule efficiently. Thus, it will slow down the training of SLFN.

4.9 Grid searching of number of hidden neurons

In this experiment, we used grid searching method to validate 15 is the optimal number of hidden neurons. We changed the number of hidden neurons from 5 to 20 with increase of 1, and keep the settings as the same as previous: use combination of MACIs and FRFEs, and use SLFN + WD as the classifier. λ is assigned to the value of 0.1. The overall accuracy of 10×10-fold cross validation changes with the number of hidden neurons, and Fig. 13 shows the curve depicting their relationship.

From Fig. 13, we can observe that the optimal number of hidden neurons is 15. Besides, the overall accuracy will decrease irregularly if the number is less than 15 or more than 15. This experiment shows the grid-searching method is effective in tuning the neural network parameters.

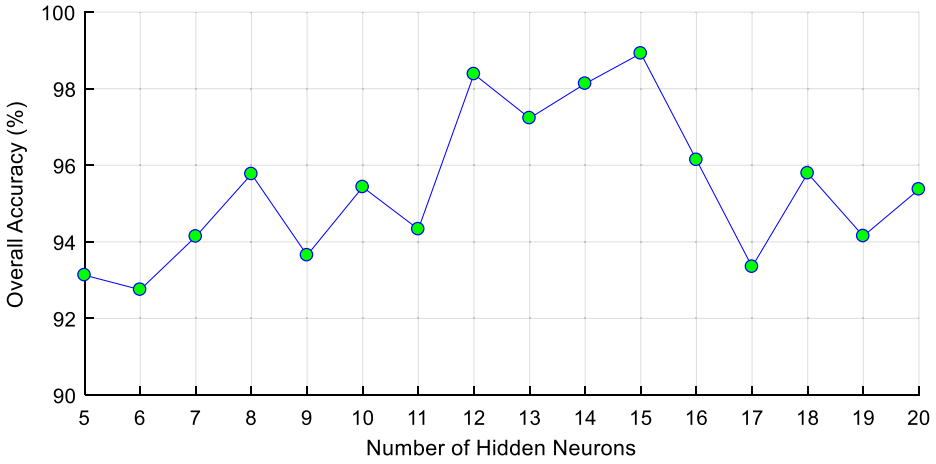

Fig. 13 Curve of overall accuracy changing with number of hidden neurons

5 Conclusion

We proposed a novel angiosperm-genus classification method based on two kinds of features: most abundant color index and fractional Fourier entropy. Weight decay was used as regularization method for the single-hidden-layer feed-forward neural network. The results showed the effectiveness of both the proposed combined feature vector, and the weight decay strategy.

This preliminary research collects three main genera (Hibiscus, Orchis, and Prunus) with various species and different photographing conditions. In the future, we will add more petal images of other angiosperm genera. We shall make tentative experiments based on other classifiers, for example, twin support vector machine and convolutional neural network.

Acknowledgements This paper was supported by Natural Science Foundation of Jiangsu Province (BK20150983), Natural Science Foundation of China (61602250).

Compliance with Ethical Standards

Conflicts of Interest The authors declare no conflict of interest involved in this paper.

References

1. Abdelali HA et al (2016) Fast and robust object tracking via accept-reject color histogram-based method. J Vis Commun Image Represent 34:219–229
2. Alves CT et al (2014) Antifungal activity of phenolic compounds identified in flowers from North Eastern Portugal against Candida species. Future Microbiol 9:139–146
3. Bartrina I et al (2011) Cytokinin regulates the activity of reproductive meristems, flower organ size, ovule formation, and thus seed yield in arabidopsis thaliana. Plant Cell 23:69–80
4. Bhalke DG et al (2016) Automatic musical instrument classification using fractional fourier transform based- MFCC features and counter propagation neural network. J Intell Inf Syst 46:425–446
5. Cattani C, Rao R (2016) Tea category identification using a novel fractional fourier entropy and jaya algorithm. Entropy 18:77
6. Chamberlain CJ (1961) Gymnosperms: structure and evolution. University of Chicago Press, Chicago
7. Chen S et al (2015) Magnetic resonance brain image classification based on weighted-type fractional Fourier transform and nonparallel support vector machine. Int J Imaging Syst Technol 25:317–327
8. Cheng K, Tan X (2014) Sparse representations based attribute learning for flower classification. Neurocomputing 145:416–426
9. Connor P et al (2015) A biological mechanism for bayesian feature selection: weight decay and raising the LASSO. Neural Netw 67:121–130
10. Elgamel SA (2016) Using empirical mode decomposition and fractional Fourier transform-segment filtering algorithm to suppress high-power interference in non-linear chirp radars. IET Radar Sonar Navig 10:892–900
11. Gaxiola F et al (2016) Optimization of type-2 fuzzy weights in backpropagation learning for neural networks using GAs and PSO. Appl Soft Comput 38:860–871
12. Goulianas K et al (2016) An adaptive learning rate backpropagation-type neural network for solving n x n systems on nonlinear algebraic equations. Math Meth Appl Sci 39:2602–2616
13. Grzeszczuk M et al (2016) Biological value of various edible flower species. Acta Sci Pol-Hortorum Cultus 15:109–119

14. Guru DS et al (2010) Texture features and KNN in classification of flower images. Int J Comput Appl S1: 21–29
15. Guru DS et al (2011) Textural features in flower classification. Math Comput Model 54:1030–1036
16. Ji G (2014) Fruit classification using computer vision and feedforward neural network. J. Food Eng 143: 167–177
17. Jiang P, Chen JJ (2016) Displacement prediction of landslide based on generalized regression neural networks with K-fold cross-validation. Neurocomputing 198:40–47
18. Laber EB, Murphy SA (2011) Adaptive confidence intervals for the test error in classification. J Am Stat Assoc 106:904–913
19. Lee HH et al (2015) Mobile-based flower species recognition in the natural environment. Electron Lett 51:2
20. Leung ACS et al (2012) Decouple implementation of weight decay for recursive least square. Neural Comput & Applic 21:1709–1716
21. Maparyan L (2016) Seeds of light, flowers of power, fruits of change ecowomanism as spiritualized ecological praxis. Worldviews 20:48–63
22. Nilsback ME, Zisserman A (2006) A visual vocabulary for flower classification. In: IEEE Computer Society Conference on Computer Vision and Pattern Recognition (CVPR'06), IEEE, pp 1447–1454
23. Nilsback ME, Zisserman A (2008) Automated flower classification over a large number of classes. In: Sixth Indian Conference on Computer Vision, Graphics & Image Processing, IEEE, pp 722–729
24. Pacifico LDS, Ludermir TB (2012) Improved group search optimization based on opposite populations for feedforward networks training with weight decay. In: International Conference on Systems, Man, And Cybernetics, IEEE, Seoul, pp 474–479
25. Pwasong A, Sathasivam S (2016) A new hybrid quadratic regression and cascade forward backpropagation neural network. Neurocomputing 182:197–209
26. Rudall PJ et al (2009) Nonflowers near the base of extant angiosperms? spatiotemporal arrangement of organs in reproductive units of hydatellaceae and its bearing on the origin of the flower. Am J Bot 96:67–82
27. Rundo L et al (2016) Combining split-and-merge and multi-seed region growing algorithms for uterine fibroid segmentation in MRgFUS treatments. Med Biol Eng Comput 54:1071–1084
28. Saitoh T, et al (2004) Automatic recognition of blooming flowers. In: 17th International Conference on Pattern Recognition. IEEE, Cambridge, pp 27–30
29. Sambamurty AVSS (2010) Taxonomy of angiosperms. I.K. International Publishing House Pvt. Limited, Delhi
30. Sari YA, Suciati N (2014) Flower classification using combined *a*b**Color and dractal-based texture feature. Int J Hybrid Inf Technol 7:357–368
31. Sasaki K, Ohtsubo N (2016) Promotion of Efficient Molecular Breeding Using Chimeric Repressors in Ornamental Flowers. Jarq - Jpn Agric Res Q 50:79–86
32. Spyropoulos A, Mordohai P (2016) Correctness prediction, accuracy improvement and generalization of stereo matching using supervised learning. Int J Comput Vis 118:300–318
33. Stemplewski S, Polewski M (2016) Computer-aided diagnosis system with backpropagation artificial neural network-improving human readers performance. In: Wilimowska Z, Borzemski L, Grzech A, Swiatek J (eds) Information Systems Architecture And Technology, vol. 432. Springer-Verlag Berlin, Berlin, pp 197–205
34. Sun Y (2016) A multilayer perceptron based smart pathological brain detection system by fractional fourier entropy. J Med Syst 40:173
35. Vasudevan H et al (2015) Delaunay triangulation on skeleton of flowers for classification. Procedia Computer Science 45:226–235
36. Yang J (2015) Identification of green, oolong and black teas in China via wavelet packet entropy and fuzzy support vector machine. Entropy 17:6663–6682
37. Yang X et al (2015) Pathological brain detection by a novel image feature—fractional fourier entropy. Entropy 17:8278–8296
38. Yeh IC et al (2012) Minimum risk neural networks and weight decay technique. In: Huang DS, Gupta P, Zhang X, Premaratne P (eds) Emerging Intelligent Computing Technology And Applications, vol. 304. Springer-Verlag Berlin, Berlin, pp 10–16
39. Yuan ZW, Zhang J (2016) Feature extraction and image retrieval based on AlexNet. Proc SPIE 10033: 100330E

Yu-Dong Zhang received his Ph.D. degree from Southeast University at 2010. He worded as postdoc from 2010 to 2012, and a research scientist from 2012 to 2013 at Columbia University. He worked as a full professor in Nanjing Normal University from 2013 to 2016. At present he worked as a professor in Henan Polytechnic University. He served as IEEE senior member and ACM senior member. He is included in "Most Cited Chinese researchers (Computer Science)" from 2015 to 2017. He won the "Emerald Citation of Excellence 2017". He is elected as the "Bentham Ambassador".

Junding Sun received B.S. degree in computer application and M.S. degree in control theory and control engineering from Henan Polytechnic University, Jiaozuo, Henan, China, in 1998 and 2001, respectively. He received his Ph.D. degree in computer application from Xidian University in 2005. His major interests are image processing, image retrieval, pattern recognition, and multimedia application.